Actively Perceiving and Responsive Soft Robots Enabled by Self-Powered, Highly Extensible, and Highly Sensitive Triboelectric Proximity- and Pressure-Sensing Skins

Ying-Chih Lai, Jianan Deng, Ruiyuan Liu, Yung-Chi Hsiao, Steven L. Zhang, Wenbo Peng, Hsing-Mei Wu, Xingfu Wang, and Zhong Lin Wang*

Robots that can move, feel, and respond like organisms will bring revolutionary impact to today's technologies. Soft robots with organism-like adaptive bodies have shown great potential in vast robot–human and robot–environment applications. Developing skin-like sensory devices allows them to naturally sense and interact with environment. Also, it would be better if the capabilities to feel can be active, like real skin. However, challenges in the complicated structures, incompatible moduli, poor stretchability and sensitivity, large driving voltage, and power dissipation hinder applicability of conventional technologies. Here, various actively perceivable and responsive soft robots are enabled by self-powered active triboelectric robotic skins (tribo-skins) that simultaneously possess excellent stretchability and excellent sensitivity in the low-pressure regime. The tribo-skins can actively sense proximity, contact, and pressure to external stimuli via self-generating electricity. The driving energy comes from a natural triboelectrification effect involving the cooperation of contact electrification and electrostatic induction. The perfect integration of the tribo-skins and soft actuators enables soft robots to perform various actively sensing and interactive tasks including actively perceiving their muscle motions, working states, textile's dampness, and even subtle human physiological signals. Moreover, the self-generating signals can drive optoelectronic devices for visual communication and be processed for diverse sophisticated uses.

Robotics will make a revolutionary impact to human life, ranging from industry, service, exploration, to healthcare and medical treatment.[1,2] Current challenges include robotics' perception and cognition, interaction with human, and freedom of movement.[1,2] Soft robots inspired from organisms' body have shown great potential.[2–4] As compared to rigid counterparts, soft robots constructed from compliant and extendable materials provide safer and more robust interaction with human, bridging the gap between machines and people.[5–8] Their deformable and muscle-like actuations enable to adapt unpredictable environments and relatively free in movement.[9,10] Those unique merits can greatly broaden robotic applications in robot–human and robot–environment interactions which were not possible before.[2–5] However, lack of suitable electronics that can be deployed on their deforming bodies for sensing, interacting, and feedback-controlling seriously limits their practical and tremendous potential.[1–7] Until now, there are relatively few reports that can practically enable soft robots to sense external and internal stimuli,[6,7,11] and no soft robot can actively perceive and respond to stimuli via self-generating electricity.

In organisms, skins serve as not only surface protections with excellent mechanical attributes such as flexibility, stretchability, and compliance but also the largest organs to actively perceive environmental information including touch, pressure, moisture, and so on. Electronic devices mimicking skins, that is, electronic skins, have shown the promise of facilitating advancement in robotics, flexible electronics, and medical technologies.[12–14] However, developing skin-like sensors that can work on soft robots is extraordinarily difficult due to their continuously deforming and stretching bodies. List of challenges include complicated device structures, scant stretchability, poor performances, and incompatible moduli.[6,7,11–14] Also, flexible passive sensors (e.g., resistive/capacitive/optical-type) require to be continuously preprovided large driving voltage (normally 1–10 V) or optical signals to drive them operation.[6,7,11–16] The

Prof. Y.-C. Lai, Dr. J. Deng, Dr. R. Liu, S. L. Zhang, Prof. W. Peng, Prof. X. Wang, Prof. Z. L. Wang
School of Materials Science and Engineering
Georgia Institute of Technology
Atlanta, GA 30332, USA
E-mail: zhong.wang@mse.gatech.edu
Prof. Y.-C. Lai, Y.-C. Hsiao, H.-M. Wu
Department of Materials Science and Engineering
National Chung Hsing University
Taichung 40227, Taiwan
Prof. Z. L. Wang
Beijing Institute of Nanoenergy and Nanosystems
Chinese Academy of Sciences
National Center for Nanoscience and Technology (NCNST)
Beijing 100083, P. R. China

The ORCID identification number(s) for the author(s) of this article can be found under https://doi.org/10.1002/adma.201801114.

large driving voltage for each sensor and the huge amount of power consumption for large-area and multiplexing sensing matrix hinder the applicability.[12–14] Especially, the heavy and rigid power source with limited capacity is another issue for autonomous soft robots.[3,4,17,18]

In order to develop crucial sensory apparatus for soft robots, it is necessary to find other technology to circumvent the limitations of conventional sensors.[1] Triboelectric effect is a natural phenomenon that a material becomes electrically charged after it contacts another material because of different electronegativities.[19–21] The presence of triboelectric charges on the dielectric surface enables to create an electric potential for driving free electrons to flow in external circuit. Based on the principle, triboelectric nanogenerators and self-powered sensors were invented as effective ways to convert mechanical energy into electricity for energy and sensing purposes.[20–24] Series efforts have been made to develop flexible triboelectric pressure sensors. However, there is always a trade-off between the mechanical attributes, that is, flexibility and stretchability, and device performances, that is, pressure sensitivity and lowest detection limit, for triboelectric pressure sensors.[24–30] For example, for single-electrode-mode triboelectric sensor,[27–30] a hydrogel-based one was reported with high stretchability about 1000%; however, it lacked for pressure sensitivity (0.013 kPa^{-1}, from contact of nylon and poly(dimethylsiloxane)) and only responded to lager pressure (>1300 Pa).[27] Despite a two-connected-tribo-layer, the contact-separation-mode triboelectric sensor showed high sensitivity to 0.31 kPa^{-1} (from contact of silver nanocomposite and polydimethylsiloxane); however, its complicated double-layer structure and the required gaps/spacers limited its flexibility and stretchability.[24–26] Considering the uses in soft robots, they also suffer from mismatched moduli and incompatible with fluidic actuators. Till now, there is no triboelectric sensor that can practically employ in soft robots to perform sensing tasks.

Here, for the first time, various kinds of soft robots have been demonstrated to actively perceive and respond to external stimuli and internal motions via self-generating electricity. They are enabled by self-powered, highly stretchable, and highly sensitive triboelectric skins that can actively sense proximity and pressure via triboelectrification effect. The tribo-skins with triangular-microprism surfaces simultaneously possess excellent stretchability to 100% strain and excellent sensitivity to 0.29 kPa^{-1} (9.54 V kPa^{-1}) (from contact of Eco-flex silicone rubber and glass) in low-pressure regime (<5 kPa) and outstanding lowest detection limit to 63 Pa. Due to the merits in all aspects, the tribo-skins can be monolithically integrated into pneumatic actuators and enable soft robots to perform various actively perceiving and responding tasks. For a conscious gripper, it can actively be aware of different actions in moving an object including approaching, grabbing, lifting, lowering, and even the accident of dropping off the objects. A perceivable robot-finger can detect if a baby wet the pants. And, a conscious robotic crawler enables to perceive its muscle motions during undulating gaits and detect very subtle human physiological signals. Such robots with large-area tribo-skins have been demonstrated for actively multiplexing-sensing uses. Moreover, the actively responding signals can directly drive optoelectronic components for intuitive communication and be further

processed for more sophisticated uses such as answering with sound, light, phrases, and so on. The presented tribo-skins that are self-powered, highly sensitive, highly stretchable, and practicable can meet a wide range of applications where soft interactive interfaces are needed. And, the first achievements in the actively perceiving and responsive soft robots can push the boundaries of artificial intelligences, soft robotics, as well as their vast related applications.

Figure 1a illustrates schematic fabrication. Details are in the Supporting Information. Percolating silver-flake network was used as the extendable conductor. Super-soft yet tough Eco-flex 00-30 silicone rubbers were used for the encapsulated and triboelectric materials as well as pneumatic actuators. Triangular-microprism structures were constructed on rubber's surface as pressure-sensitive triboelectric layer. Through homogeneous integration, the tribo-skins were integrally formed into various functional soft robots in a piece. Figure 1b reveals a scanning electron microscopy (SEM) image of the laid silver flakes, showing lots of voids that enabled rubber to penetrate into the silver-flake matrix. After processing, the conducting matrix was sandwiched between elastomers (Figure 1c). Figure 1d,e shows side-view and top-view SEM images of the triangular microprisms, respectively. The height and width of the triangular microprisms are 1.24 mm and 1.64 mm, respectively. The word of "micro" prisms means that the pressure-sensitive structures are very "tiny" as compared to the whole surface. The scales and shapes of the sensing structures differ from the ones in the previous two-layer-contact-separation-mode tribo-sensor because of the difference in the requirements for the scales of the sensing structures and the corresponding fabrication methods.[24] Silicone rubber (Young's moduli, ≈40 kPa) is much softer than polydimethylsiloxane (Young's moduli, ≈2 MPa).[3,31] A small pressing force can easily flatten the surface sensing structures if the sensing structures are patterned by a nano- or micrometer-structure mold. The mold for our single-electrode tribo-skin was fabricated by laser grinding to obtain larger cavities. Their shapes were limited by the linear motor of laser grinding machine and the sizes of laser beam. Figure 1f presents the tribo-skin with demonstrating its excellent deformability and mechanical compliance, including being folded, stretched, and twisted.

Figure 1g illustrates schematic working mechanism of the self-powered tribo-skin. Comparing to passive sensors, the driving energy of the tribo-skin comes from triboelectrification effect, involving a cooperation of contact electrification and electrostatic induction.[19–21] Rubber with the highest electron affinity represents an excellent triboelectrically negative material.[21] When an object comes in contact with the tribo-skin, electrons shift from the object's surface to rubber's surface due to the difference in electronegativity. As the object is leaving away, the two oppositely charged surfaces become separated and create a potential difference. The unscreened negative charges on the rubber surface drive free electrons flowing from the embedded silver flakes to the ground and induce the accumulation of positive charges in the electrode, thus generating a current and voltage output. When the object is far away, an electrostatic equilibrium is attained and electrons stop moving. As the object approaches again, the separated distance between the tribo-skin and object as well as their potential difference

**ADVANCED
SCIENCE NEWS**

www.advancedsciencenews.com

**ADVANCED
MATERIALS**

www.advmat.de
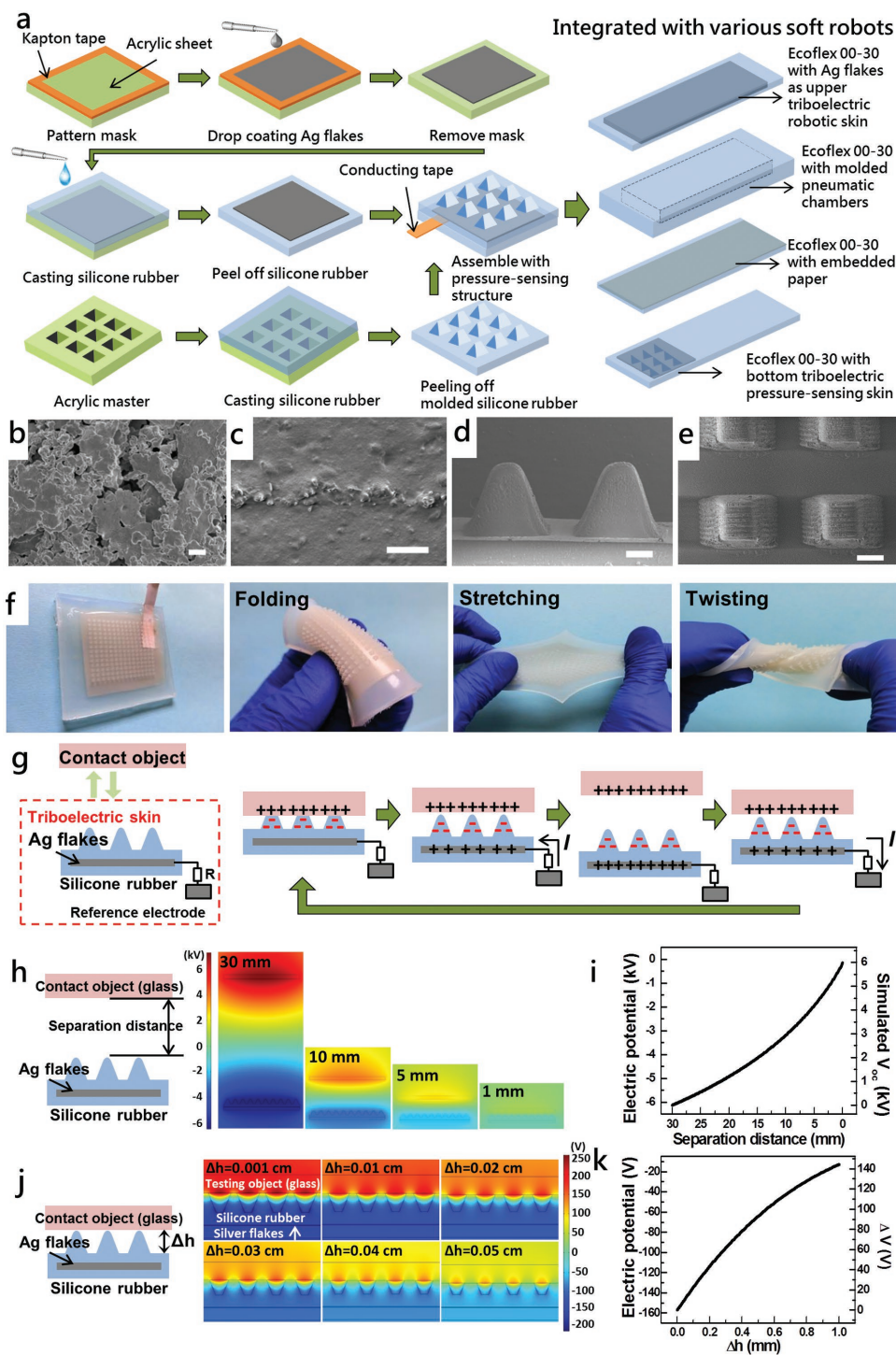
Figure 1. Deformable and mechanically compliant tribo-skins. a) Schematic fabrication of tribo-skin and exploded view of conscious soft robot showing its four-layer Eco-flex 00-30 structure consisting of tribo-skins and pneumatic actuators. b) SEM image of silver-flake matrix (Scale bar = 1 µm). c) Cross-view SEM image of sandwiched silver-flake matrix (Scale bar = 50 µm). d) Front-view and e) top-view SEM images of triangular microprisms (Scale bar = 0.5 mm). f) Photos of as-prepared device with demonstrations of being different mechanical deformations, including folding, stretching, and twisting. g) Schematic illustration of working mechanism. h) Simulated electric potential distribution when object approaching tribo-skin. i) Simulated electric potential of embedded electrode and generated V_{oc} at different separation distance between object and tribo-skin. j) Simulated electric potential distribution at different deformation depth (Δh) of triangular microprisms. k) Simulated electric potential of embedded electrode and its increased output at different deformation depth pressed by object.

decrease. This process leads to a reverse electron flow from the ground to the embedded electrode and generates a voltage in the opposite direction. Experiencing different pressures, different corresponding contact areas and deformation depth are formed on the triangular microprisms, resulting in pressure-dependence charges in the silver flakes and pressure-dependence outputs to external circuits.

Finite element simulations about the tribo-skin's electric potential distribution during approaching and touching of an object are shown in Figure 1h–k. Detailed simulated methods are given in Text S1 (Supporting Information). The model was set at open-circuit condition. Simulated open-circuit voltage (V_{oc}) was defined as zero when the object was 30 mm away, which was the same as the measurement setup. It can be found that the electric potential of the embedded electrode and the simulated outputs increase as the object approaches (Figure 1h,i) and presses (Figure 1j,k) the triangular microprisms of the device. Further description about the mechanism of sensing static contact pressure is described in Text S2 (Supporting Information).

A piece of glass was set at 30 mm away and used as the contact object for a standard test. **Figure 2**a shows generated V_{oc} when the object approached the device, which is corresponding to the trend of simulation. The contactless output originated

from the change of the local electrostatic field on the rubber surface during the object approached.[29,32] The difference in scale between the numerical and experimental results is discussed in Text S3 (Supporting Information).

Figure 2b–d shows real-time generated V_{oc}, transferred charges (Q_{tr}), and short-circuit current (I_{sc}) responding to different contact pressures, respectively. Produced V_{oc} increased as contact pressure increased and recovered to a based line after releasing the pressure (Figure 2b). Similar to V_{oc}, the amount of Q_{tr} was obtained when the device was pressed and returned to zero after relieving contact pressure (Figure 2c). Generated I_{sc} showed dynamic alternating-current responses to the instant moment of applying and releasing contact pressures (Figure 2d). Detailed output signals are described in Figure S1a–c (Supporting Information).

Figure 2e shows the statistic V_{oc} from the devices with no and different-sized triangular-microprism structures (Q_{tr} and I_{sc} are in Figure S2a,b, Supporting Information). The results show that the outputs from the devices with middle-sized triangular-microprism structures (height = 1.24 mm; width = 1.64 mm) showed much better sensitivity and resolution than the others in low pressure (<5 kPa) regime. Sensitivity of 0.29 kPa^{-1} (9.54 V kPa^{-1}) was obtained in low-pressure (<5 kPa) regime (Figure S3, Supporting Information), which is far higher than
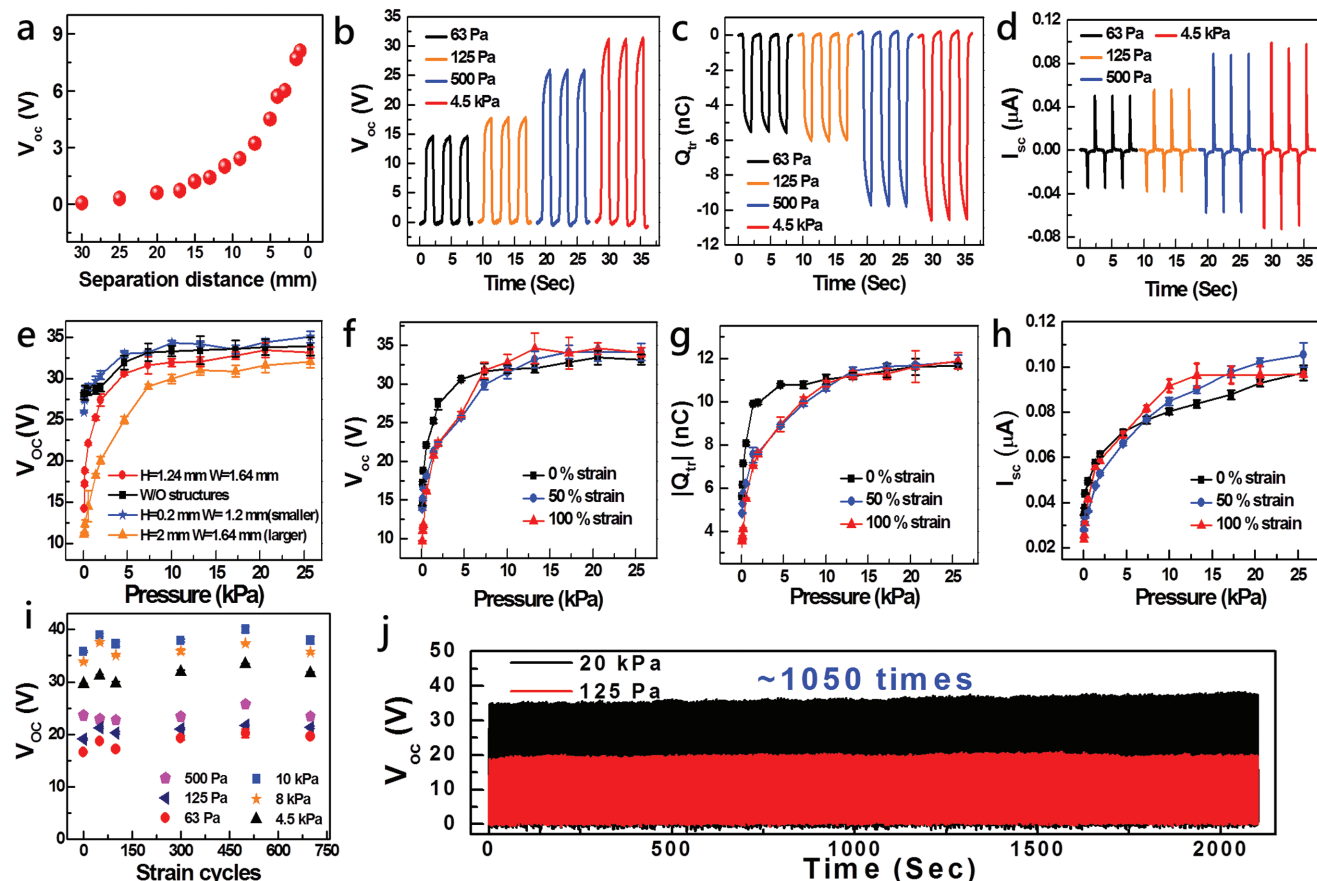
Figure 2. Performance of tribo-skins. a) Generated V_{oc} to the separation distance. b,c) Real-time generated V_{oc}, Q_{tr}, and I_{sc} to different contact pressures, respectively. e) Generated V_{oc} of devices with no and different-sized triangular microprisms to different pressures (H: height and W: width of triangular microprisms). f–h) Generated V_{oc}, Q_{tr}, and I_{sc} to difference pressures when the device with middle-sized triangular microprisms were stretched. i) V_{oc} to different pressure after device was repeatedly elongated at 50% strain. j) V_{oc} during cyclically loading and unloading two pressures of 20 kPa and 125 Pa.

previous reported stretchable triboelectric skin.[27] The device can detect pressure as low as 63 Pa, which is more favorable than previously reported stretchable capacitive soft-robotic skin that can only sense pressure >900 Pa.[7] A discussion about the devices with different-sized triangular-microprism structures is given in Text S4 (Supporting Information). The extraordinary sensitivity and resolution in low-pressure regime are important merits that can put soft robots into full play in human–robots and in situ palpation applications such as detecting subtle touch and even slight physiological signals like pulses.[33,34] Such demonstrations are presented in later sections. For pressures beyond 5 kPa, the outputs grew gently.

Figure 2f–h shows outputs responding to different pressures when the device was elongated to 50 and 100% strains, indicating that the device can well retain its sensing function even when it was experiencing strain. Compared to previous passive or triboelectric pressure sensors,[24–30,32] the presented device showed a remarkable capability of not only possessing excellent stretchability but also simultaneously keeping outstanding sensitivity. The breakthrough comes from two facts: (i) the device was fabricated by a composition of inherently extensible materials and construction; (ii) the shapes of triangular microprisms on rubber's surface can be nearly maintained even when the device was deformed. Figure S4 (Supporting Information) describes the stress distribution of one triangular-microprism unit when the device was stretched to 50% strain, indicating that the stresses were mostly concentrated on the substrate and the base of the triangular microprism. The relatively less stress on the triangular microprism enables the shape of pressure-sensitive structure to be maintained.

It was observed that outputs in low-pressure regime decreased as strain increased; however, outputs in high-pressure regime were nearly similar between different strains. This is because partial triangular-microprism structures were moved out from the fixed testing area during stretching the device. When applied pressures were small, fewer contact areas were formed with the triangular microprisms, leading to the lower outputs. Thus, in low-pressure regime, outputs were dominated by the underlying sensing structures. When the pressures were increased to high-pressure regime, the pressure-sensitive triangular microprisms were rammed down, and the object fully touched the rubber. Consequently, in high-pressure regime, outputs were dominated by the fixed object area.

The stability after repeated elongation was investigated through repeatedly stretching the device to 50% strain and measuring its outputs to different pressure. Figure 2i reveals that the responses show no significant degradation within 700 times stretching. The excellent mechanical stability is ascribed to the symmetrical and integrated rubber/silver flakes/rubber structure which can avoid moduli-mismatched buckling phenomenon between the elastics and embedded conducting matrix.[35]

The long-term stability was examined through continuously loading and unloading two pressures of 20 kPa (strong pressure) and 125 Pa (small pressure). In Figure 2j, no obvious reductions of outputs were found after applying the two pressures separately for over 1000 times, through which the long-term stability can be confirmed. Figure S5 (Supporting Information) demonstrates that the device can retain the capability to sense a subtle pressure (63 Pa) even after applying a huge force (stepped by an ≈82 kg (≈803 N) man), indicating its excellent strength.

To investigate the effect of contact speed, applied pressures were set at different acceleration. It was found that V_{oc} (**Figure 3**a) and Q_{tr} (Figure S6, Supporting Information) were nearly independent of the contact speed; on the contrary, I_{sc} showed obvious dependence on object's speed (Figure 3b). This is because the current flow came from induced charges in silver-flake matrix per second.[24] The term of time in denominator leads to the result that shorter contact time rendered higher current. Thus, generated V_{oc} and Q_{tr} can be favored to sense forces without considering contact speed, while I_{sc} can be used for sensing acceleration.[24] Because the outputs originated from the change of rubber's triboelectric field in the vertical direction, the device showed no obvious response to deformations of bending and extending as compared with pressing (Figure S7a,b, Supporting Information).

The tribo-skin can work on different loading circuit in practical uses. The output voltages depending on different resistances of circuits are investigated in Figure 3c. Its output powers to loads are shown in Figure S8 (Supporting Information).

Figure 3d and Figure S9a,b (Supporting Information) show outputs responding to different contacted materials, indicating that different contact materials can induce different levels of outputs.[27–30,32] Also, the device can respond to both insulating and conductive surfaces. A proximity test to conductive surface is shown in Figure S10 (Supporting Information). Outputs responding to contact materials are common features for single-electrode-mode triboelectric-type electronic skins.[27–30,32] A discussion about the uses of the sensing capability in soft robots is given in Text S5 (Supporting Information). It was found that the contact to a wet textile makes outputs drastically decrease to a quite low level (Figure 3d and Figure S9a,b, Supporting Information). This is because water molecules on the wet textile reduced triboelectric charges on the rubber surfaces.[36] A quantizing examination is shown in Figure 3e. Recovery time to different water contents of the contacted textiles was investigated in Figure 3f. The effects of environment factors are shown in Figure S11a,b (Supporting Information). The results indicate that the outputs reveal no significant difference in the normal environmental condition (295–323 K; 40–60% RH).

The inherent stretchability and compatible materials enable the tribo-skins to integrally embed in soft robots as active robotic skins that can perceive and respond to stimuli via self-generated electricity. A perceivable soft gripper was first demonstrated (**Figure 4**a and Figure S12, Supporting Information).[37] The tribo-skins were monolithically integrated onto the two fingers of the gripper (Figure 4b). Its circuit is in Figure S13 (Supporting Information). Figure 4c and Movie S1 (Supporting Information) show the outputs responding to different steps in grabbing an object. Initially, both right and left tribo-skins were at low-voltage regimes. As the fingers approached the object, generated voltages from individual sensor started to rise up, corresponding to proximity sensing of the tribo-skins. Till the gripper contacted and compressed the object, both outputs were achieved to the maximum values, corresponding to contact and pressure sensing. When the gripper grabbed up the
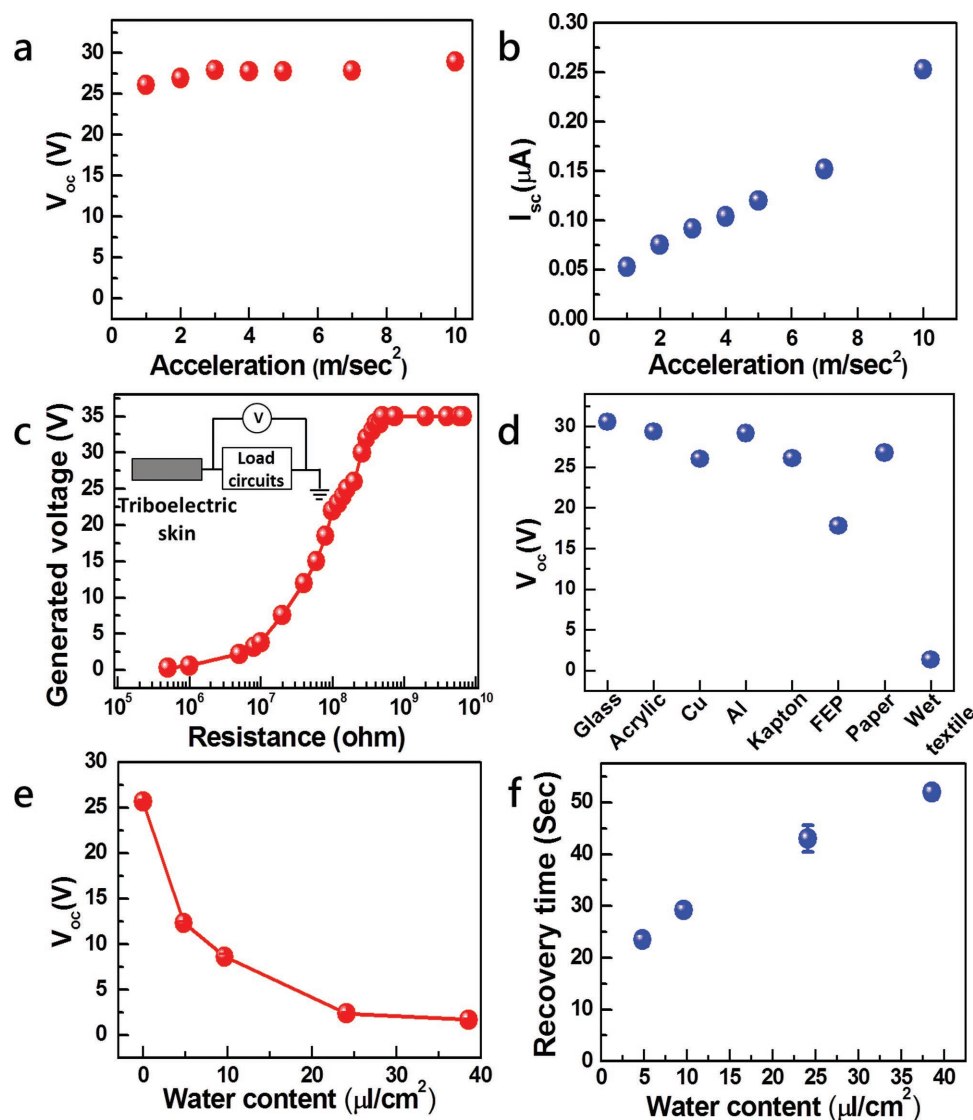
Figure 3. Characteristics of tribo-skins. a,b) Generated V_{oc} and I_{sc} to different acceleration of contact object (glass), respectively. c) Generated voltage to different load resistances. d) Generated V_{oc} to different contacted materials. e) Generated V_{oc} to different water content of textiles. f) Recovery time of tribo-skin after touching wet textiles with different water contents.

object, outputs slightly decreased and kept at lower voltages. The slight decrease was attributed to the reason that partial potentials were contributed from the electrostatic field to the desk. The responses were further investigated when the object was suddenly dropped from the gripper. When this situation was happened, outputs drastically declined to the lowest levels, corresponding to separation between the object and tribo-skins. The result shows that the actively generated signals enable the gripper to perceive different actions in grabbing an object and be aware of the accident of dropping off the goods, indicating their promising uses in industrial robotics for monitoring and feedback controlling.

Soft robots show superiority in interacting with nonconventional objects due to their adaptive bodies.[2–5] The excellent integration of the compliant tribo-skins and soft actuators enables to actively perceive unpredictable environment without sacrificing the merits of both. To prove this, the perceivable

gripper was tested its outputs as holding and shaking an irregular baby doll's hand (Figure 4d). In Figure 4e and Movie S2 (Supporting Information), voltages were generated when the gripper approached the doll's hand and reached to the maximum values when it held the hand, corresponding to proximity and pressure sensing of the tribo-skins. While the gripper shook the hand up and down, produced voltages responded the movement correspondingly. After the gripper released the hand and left, outputs recovered to baseline values. The results show that the perfect integration can well retain both compliant and shape-adaptive features.

The tribo-skin can discern dampness of contact objects. To demonstrate the uses in robotic applications, a perceiving robotic finger was designed to detect the moisture of baby's pants (Figure 4f, Figures S14 and S15, Supporting Information). The investigation of a doll's pants was tested in two conditions which were wet and dry pants to simulate the case that a

**ADVANCED
SCIENCE NEWS**
www.advancedsciencenews.com

**ADVANCED
MATERIALS**
www.advmat.de
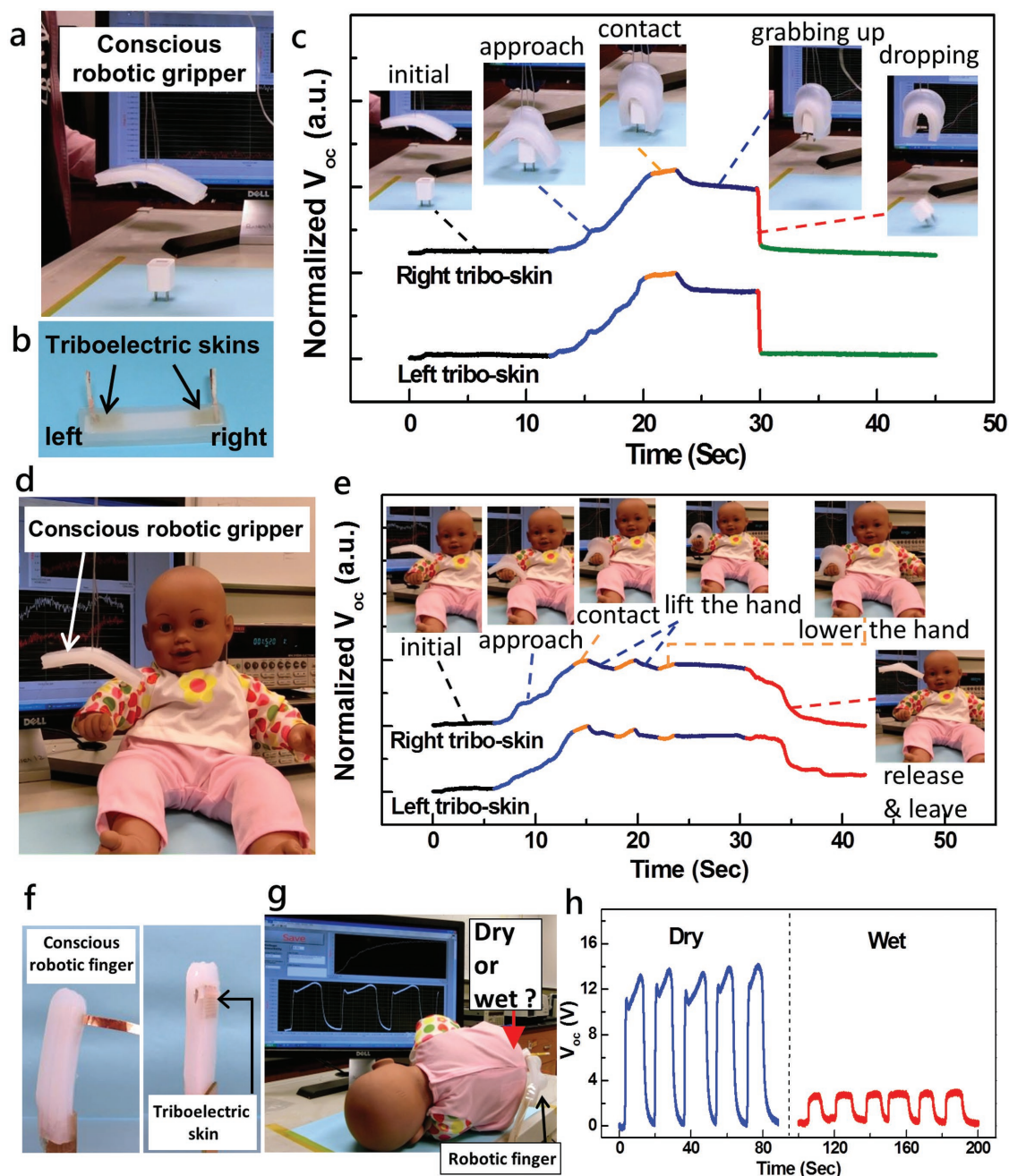
Figure 4. Tribo-skins enable soft robotic gripper and finger to actively perceive working states and textile dampness. a) Image of conscious soft gripper. b) Image of abdomen of robotic gripper with indicating tribo-skins. c) Real-time outputs of right and left tribo-skins when conscious gripper grabbed and dropped an object. d) Image of conscious gripper to hold the doll's hand. e) Real-time outputs of right and left tribo-skins when conscious gripper held doll's hand. f) Image of conscious robotic finger (left) and tribo-skin (right). g) Image of detecting the dampness of the baby doll's pants. h) Real-time outputs of conscious finger when the baby doll's pants were dry and wet.

baby wet his/her pants (Figure 4g and Movie S3, Supporting Information). Figure 4h shows the outputs responding to the two states. The higher and lower voltages indicated the dry and wet pants, respectively. These results are corresponded to the results in Figure 3e.

Next, the pressure-sensitive tribo-skin was embedded on the abdomen of a caterpillar-like crawling robot and tested its capability. The crawler was constructed from three pneumatic

actuators (**Figure 5**a and Figure S16, Supporting Information), and "one" tribo-skin was deployed on the abdomen of the first segment (Figure 5b). Its circuit is shown in Figure S17 (Supporting Information). Figure 5c illustrates the detailed output to one period of undulating gaits. The output changed with actuation of each pneumatic actuator. When the first actuator was inflated, output was at the lowest state owing to the separation between the abdominal tribo-skin and desk. As the first

**ADVANCED
SCIENCE NEWS**

www.advancedsciencenews.com

**ADVANCED
MATERIALS**

www.advmat.de
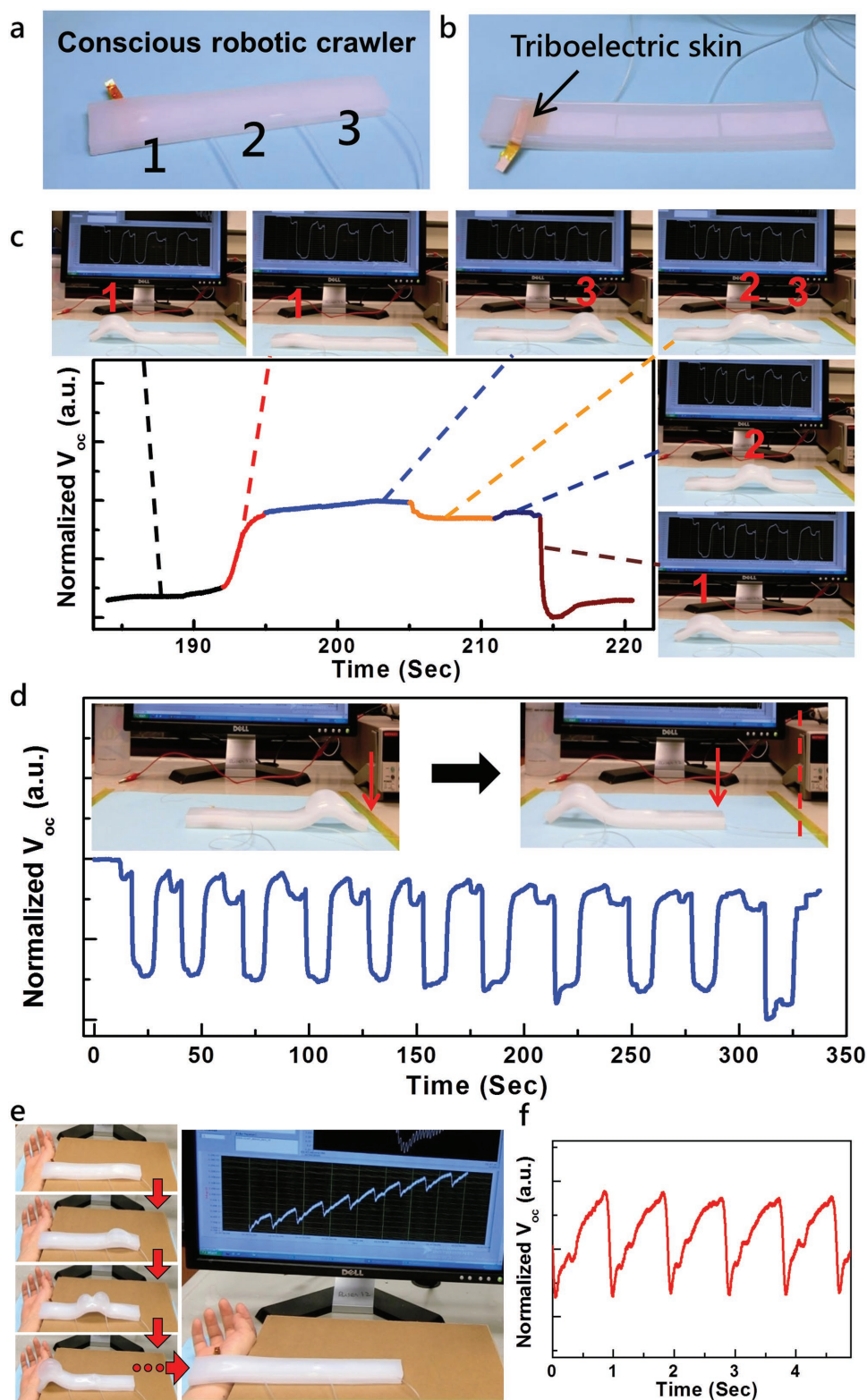
Figure 5. Conscious robotic crawler with ability to percept actuated states and sense human physiological signals. a) Image of conscious robotic crawler. b) Image of abdomen of conscious robotic crawler and tribo-skin. c) Real-time outputs of conscious crawler during one period of undulating gaits. d) Real-time outputs of conscious crawler during crawling ≈15 cm distance. e) Photos of conscious crawler moving to human wrist. f) Real-time outputs of human pulses.

**ADVANCED
SCIENCE NEWS**

www.advancedsciencenews.com

**ADVANCED
MATERIALS**

www.advmat.de

actuator was deflated and approached the desk, voltage rose up, corresponding to proximity sensing. Output reached to a high-voltage state when the first segment touched desk, corresponding to contact and pressing sensing. When the third segment was inflated, voltage reached to the highest value. This is because more force from the robot's weight was imposed on the first-segmented bottom tribo-skin to the desk while inflating the third segment. Output slightly decreased as deflating the third segment and inflating the second segment. After the third segment was fully deflated, output slightly rose up again. When the first actuation was inflated afresh, voltage was dropped to the lowest value again because decompression and separation between the abdominal sensor and desk. Outputs from bending and extending the tribo-skins have been ruled out (Figure S7a,b, Supporting Information); thus, the decreased voltage can be confirmed only from separation between the bottom tribo-skin and desk during inflating and curving the first segment. Figure 5d and Movie S4 (Supporting Information) show real-time outputs after the robot moved a distance of ≈15 cm, revealing several periods of generated potential waves. Each period of potential wave corresponded to one period of undulating gaits, indicating the tribo-skin's reliability. The soft robot's capabilities to perceive muscle motions rely on proximity, contact, or separation to other surfaces. This is because the driving energy of the robotic skin harvests from the triboelectrification effect during the motions of proximity, contact, or separation to a surface.[19–21] Soft robots are primarily used in robot–human and robot–environment interactions.[1–5] They will inevitably get proximity or contact with environment, objects, or human in practical uses.[1,2,6,7,11] These results showed that the pressure-sensitive tribo-skin enables a moving caterpillar-like robot to actively perceive its actuated/moving states, which is favorable for feedback-controlling and monitoring soft robots.[2,3,6,7]

Shape-adaptive robots provide safer interaction with human body, making their uses in human interaction and medical care highly desired.[2–4] The compliant tribo-skins with extraordinary sensitivity and resolution in low pressure enable such robotic applications with sensing ability. To demonstrate this, the perceivable crawler was controlled to move through irregular surfaces and conformally touched a human wrist to actively sense slight human physiological signals (Figure 5e and Movie S5, Supporting Information). Figure 5f depicts the human wrist's pulse signals detected from the robotic active outputs. In Movie S5 (Supporting Information), it can be found a drift of increasing voltage in the real-time outputs of the pulse signals. It is because both of the soft robot and human wrist (fat and skin) were quite soft. Young's moduli of fat and skin are ≈1 kPa and ≈10 MPa, respectively, and Young's modulus of rubber is ≈40 kPa.[3] Right after the crawler lay on the wrist to detect pulses, the fat and skin of the wrist were being pressed down progressively by the weight of soft robot, leading to a drift in pulse signals.[38] Figure S18 (Supporting Information) schematically illustrates the drift phenomena. To eliminate the effect from the progressively deforming of fat and skin, the original data were subtracted from the drift and normalized for observing pulse signals (Figure 5f). Detailed data process is illustrated in the Experimental Section. This is the first time that soft robots enable to detect human physiological signals, revealing their potential in in situ palpation and other healthcare uses.

To demonstrate large-area and multiplexing sensing uses, we further deployed multiple tribo-skins on a caterpillar-like robot. The perceivable caterpillar-like robot was constructed by three segmented pneumatic chambers. Each segment was integrated with a tribo-skin on the back (**Figure 6**a). The three back tribo-skins can not only play as human–robot interfaces but also perceive the corresponding chamber's actuation states. One triboelectric pressure-sensing skin was integrated on the first-segmented abdomen in order to perceive the bottom contact surface (Figure 6b). The deployment here represents a comprehensive sensing strategy for the soft robot that can interact with human, perceive each actuator's working state, and sense the contact surface. The circuit is shown in Figure S19 (Supporting Information). Figure 6c and Movie S6 (Supporting Information) reveal real-time outputs from the four devices in one period of undulating gait. During sequentially inflating each pneumatic chamber, the outputs corresponding to the back tribo-skins declined, which was ascribed to the increased separation distance between the tribo-skin and desk during inflating the pneumatic actuator. Consistent with previous results, the output from the bottom tribo-skin dropped sharply when the first chamber was curved. Figure 6d and Movie S7 (Supporting Information) show real-time outputs as a finger touched the moving robot, indicating not only each chamber's actuated state but also the generated electricity from touching. Figure 6e and Movie S8 (Supporting Information) reveal real-time outputs after a series of undulating gaits and touches, showing excellent stability and reliability of the tribo-skins even during continuously deforming and moving of the robot.

It is worth to discuss the four signals here. It was noted that the relative values responding to touch from the three back tribo-skins (green, red, and black curves) were at the similar scale. However, for the responses to actuator's states, the response from the first back tribo-skin (green curve) was smaller than the responses from the second and third ones (red and black curves). This is because the responses to actuator's states rely on the change of the electrostatic field between the abdominal rubber and desk during their relative movements. For the first back tribo-skin, part of the electrostatic field on the abdominal rubber was shielded by the electrode of the first-segmented bottom tribo-skin; thus, the first back tribo-skin showed smaller response to the first actuator's state. Also, the response of the bottom tribo-skin (blue curve) showed the largest response to the actuator state because the bottom tribo-skin was actual contact and separate to the desk. Its responses to touch came from its relative motions to the desk during being touched. As mentioned, the deployment is for comprehensive sensing uses of the caterpillar-like robot. The first-third back tribo-skins can interact with human and perceive the corresponding actuators' states. The bottom one can detect the contact surface. In practical uses, the multiplexing sensed signals can be separately analyzed and used.

Moreover, the actively responding output can be directly used for driving other functional components for intuitive reactions. In Figure 6f and Movie S9 (Supporting Information), the sensing signal to touch was directly used to light up a light-emitting diode (LED) for providing human-visible responses. Figure 6g and Movie S9 (Supporting Information) show a LED driven by the electricity generated from the robot's motion.

**ADVANCED
SCIENCE NEWS**

www.advancedsciencenews.com

**ADVANCED
MATERIALS**

www.advmat.de
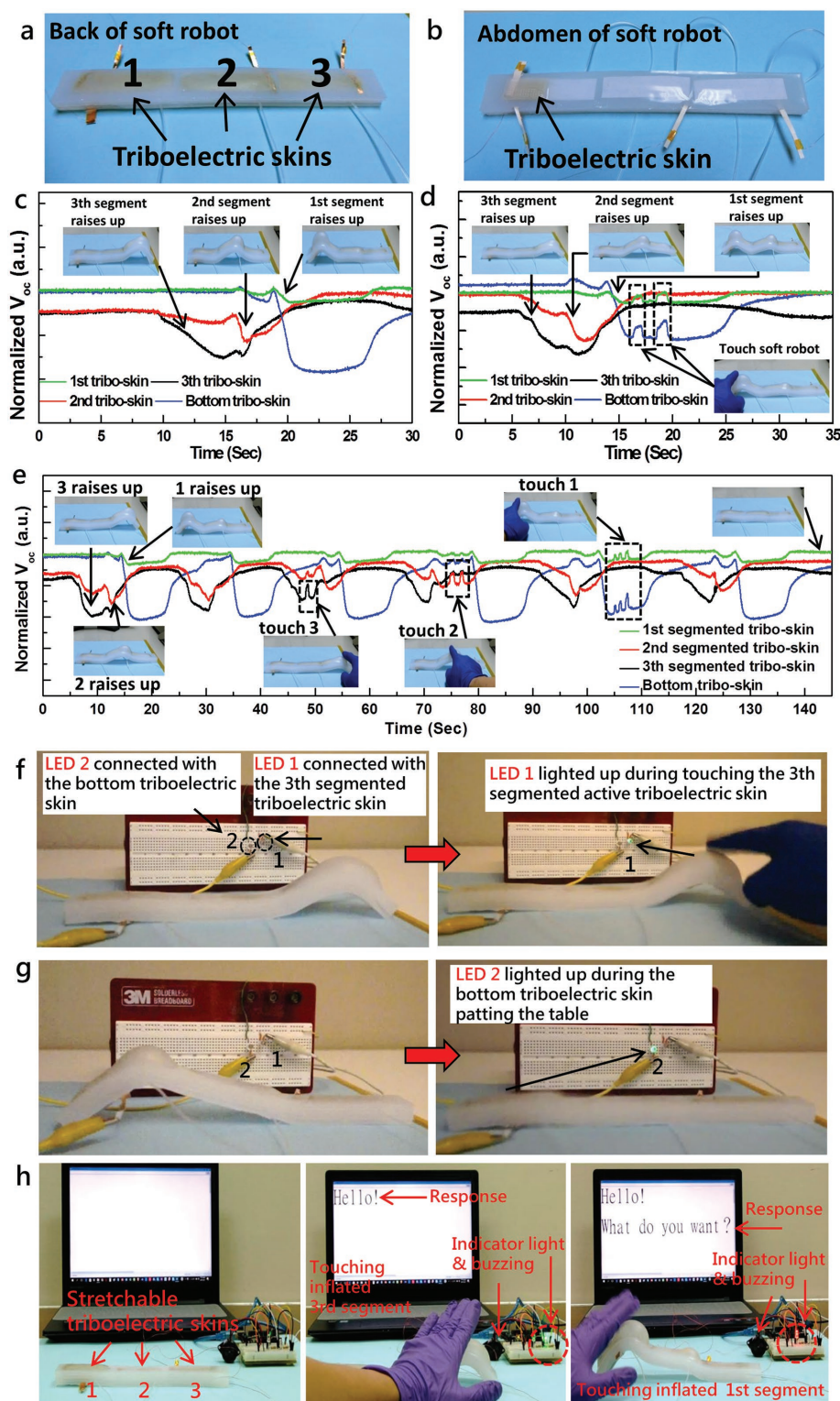
Figure 6. Large-area actively multiplexing-sensing robotic crawler and its human-interactive reaction through self-generated electricity. a) Image of back of multiplexing-sensing robotic crawler and arrows indicating three tribo-skins. b) Image of abdomen of robotic crawler and indicating bottom tribo-skin. c) Real-time outputs of multiplexing-sensing robotic crawler during one period of undulating gaits. d) Real-time outputs of multiplexing-sensing robotic crawler during one period of undulating gaits and being touched. e) Real-time generated potentials of multiplexing-sensing robotic crawler after moving 15 cm distance and being touched. f) Photos for demonstrating the use of self-generated electricity from touching to light up a LED for human-visible communication. g) Photos for demonstrating the use of self-generated electricity from muscle action. h) Photos for demonstrating the actively sensed signals processed by a computing module to reactions with human.

**ADVANCED
SCIENCE NEWS**

www.advancedsciencenews.com

**ADVANCED
MATERIALS**

www.advmat.de

These results demonstrate that the actively perceived signals enable robots to instantaneously respond to human without the need of external power sources. Several human-interactive systems have been reported by such methods.[15,21] The use of tribo-skins can simplify the systems.

Furthermore, the sensing signals can be processed by a computation module for more sophisticated reaction uses. Figure 6h and Movie S10 (Supporting Information) show a moving conscious robot that was designed to sense and respond to human touch with sounds, lights, and showing phrases. The circuit is in Figure S20 (Supporting Information). The robotic skins were connected with a signal processing module. Touching the robotic skin on the third inflated pneumatic actuator made the robot answer "Hello!" on the screen with buzzing and lighting up the green LED. And, touching the robotic skin on the first segment made the robot respond "What do you want?" with sound and red light. These results illustrate that, through a computing module, the actively perceived signals can be further processed to perform diverse robotic tasks.

Based on above results, the actively sensing signals from the perceiving soft robots can be applied in three ways. First, the signals can be directly monitored from electrometers. By this way, the perceiving soft robots have demonstrated the promising uses in monitoring and detecting their actions, checking a baby's pants conditions, palpation, and so forth (Figures 4,5, and 6a–e). Second, the signals can be used to power up optoelectronic components for visible reactions (Figure 6f,g). Third, by computing module, the signals can be further processed for diverse uses (Figure 6h).

In summary, for the first time, various actively perceiving and responsive soft robots were enabled by the highly stretchable and highly sensitive self-powered tribo-skins that can actively sense proximity, contact, and pressure by harvesting energy via triboelectrification effect. The tribo-skins can retain the sensing functionality even when they were elongated to 100% strain. The compatible features enable the tribo-skins to integrate into soft robots to actively perceive external stimuli and internal motions via self-generated electric signals. The self-generated electricity can be used not only for sensing, detecting, and monitoring but also for driving functional components for instantaneously interacting with human. Moreover, such soft robots with large-area multiplex sensing arrays have been demonstrated. The actively responding signals can also be further processed for more diverse reactions. These capabilities are all active without the need of pre-providing electricity to drive them operation. This work opens the crucial doors for the tremendous potentials of soft robots and artificial electronic-sensory skins.

Supporting Information

Supporting Information is available from the Wiley Online Library or from the author.

Acknowledgements

Conflict of Interest

The authors declare no conflict of interest.

Keywords

[1] G.-Z. Yang, J. Bellingham, P. E. Dupont, P. Fischer, L. Floridi, R. Full, N. Jacobstein, V. Kumar, M. McNutt, R. Merrifield, B. J. Nelson, B. Scassellati, M. Taddeo, R. Taylor, M. Veloso, Z. L. Wang, R. Wood, *Sci. Rob.* **2018**, *3*, eaar7650.
[2] H. Shen, *Nature* **2016**, *530*, 24.
[3] D. Rus, M. T. Tolley, *Nature* **2015**, *521*, 467.
[4] C. Laschi, B. Mazzolai, M. Cianchetti, *Sci. Rob.* **2016**, *1*, eaah3690.
[5] C. Majidi, *Soft Rob.* **2014**, *1*, 5.
[6] H. Zhao, K. O'Brien, S. Li, R. F. Shepherd, *Sci. Rob.* **2016**, *1*, eaai7529.
[7] C. Larson, B. Peele, S. Li, S. Robinson, M. Totaro, L. Beccai, B. Mazzolai, R. Shepherd, *Science* **2016**, *351*, 1071.
[8] P. Polygerinos, Z. Wang, K. C. Galloway, R. J. Wood, C. J. Walsh, *Rob. Auton. Syst.* **2015**, *73*, 135.
[9] F. Ilievski, A. D. Mazzeo, R. F. Shepherd, X. Chen, G. M. Whitesides, *Angew. Chem.* **2011**, *123*, 1930.
[10] R. F. Shepherd, F. Ilievski, W. Choi, S. A. Morin, A. A. Stokes, A. D. Mazzeo, X. Chen, M. Wang, G. M. Whitesides, *Proc. Natl. Acad. Sci. USA* **2011**, *108*, 20400.
[11] R. L. Truby, M. Wehner, A. K. Grosskopf, D. M. Vogt, S. G. Uzel, R. J. Wood, J. A. Lewis, *Adv. Mater.* **2018**, *30*, 1706383.
[12] X. Wang, L. Dong, H. Zhang, R. Yu, C. Pan, Z. L. Wang, *Adv. Sci.* **2015**, *2*, 1500169.
[13] A. Chortos, Z. Bao, *Mater. Today* **2014**, *17*, 321.
[14] A. Chortos, J. Liu, Z. Bao, *Nat. Mater.* **2016**, *15*, 937.
[15] C. Wang, D. Hwang, Z. Yu, K. Takei, J. Park, T. Chen, B. Ma, A. Javey, *Nat. Mater.* **2013**, *12*, 899.
[16] S. C. Mannsfeld, B. C. Tee, R. M. Stoltenberg, C. V. H. Chen, S. Barman, B. V. Muir, A. N. Sokolov, C. Reese, Z. Bao, *Nat. Mater.* **2010**, *9*, 859.
[17] M. Wehner, R. L. Truby, D. J. Fitzgerald, B. Mosadegh, G. M. Whitesides, J. A. Lewis, R. J. Wood, *Nature* **2016**, *536*, 451.
[18] F. Iida, C. Laschi, *Proc. Comput. Sci.* **2011**, *7*, 99.
[19] Z. L. Wang, *Mater. Today* **2017**, *20*, 74.
[20] Z. L. Wang, J. Chen, L. Lin, *Energy Environ. Sci.* **2015**, *8*, 2250.
[21] Z. L. Wang, *ACS Nano* **2013**, *7*, 9533.
[22] Z. L. Wang, *Nature* **2017**, *542*, 159.
[23] Y. C. Lai, J. Deng, S. L. Zhang, S. Niu, H. Guo, Z. L. Wang, *Adv. Funct. Mater.* **2017**, *27*, 1604462.

**ADVANCED
SCIENCE NEWS**

www.advancedsciencenews.com

**ADVANCED
MATERIALS**

www.advmat.de

[24] L. Lin, Y. Xie, S. Wang, W. Wu, S. Niu, X. Wen, Z. L. Wang, *ACS Nano* **2013**, *7*, 8266.

[25] F.-R. Fan, L. Lin, G. Zhu, W. Wu, R. Zhang, Z. L. Wang, *Nano Lett.* **2012**, *12*, 3109.

[26] K. Y. Lee, H. J. Yoon, T. Jiang, X. Wen, W. Seung, S. W. Kim, Z. L. Wang, *Adv. Energy Mater.* **2016**, *6*, 1502566.

[27] X. Pu, M. Liu, X. Chen, J. Sun, C. Du, Y. Zhang, J. Zhai, W. Hu, Z. L. Wang, *Sci. Adv.* **2017**, *3*, e1700015.

[28] K. Parida, V. Kumar, W. Jiangxin, V. Bhavanasi, R. Bendi, P. S. Lee, *Adv. Mater.* **2017**, *29*, 1702181.

[29] S. W. Chen, X. Cao, N. Wang, L. Ma, H. R. Zhu, M. Willander, Y. Jie, Z. L. Wang, *Adv. Energy Mater.* **2017**, *7*, 1601255.

[30] X. Wang, H. Zhang, L. Dong, X. Han, W. Du, J. Zhai, C. Pan, Z. L. Wang, *Adv. Mater.* **2016**, *28*, 2896.

[31] I. Johnston, D. McCluskey, C. Tan, M. Tracey, *J. Micromech. Microeng.* **2014**, *24*, 035017.

[32] G. Zhu, W. Q. Yang, T. Zhang, Q. Jing, J. Chen, Y. S. Zhou, P. Bai, Z. L. Wang, *Nano Lett.* **2014**, *14*, 3208.

[33] L. Pan, A. Chortos, G. Yu, Y. Wang, S. Isaacson, R. Allen, Y. Shi, R. Dauskardt, Z. Bao, *Nat. Commun.* **2014**, *5*, 3002.

[34] G. Schwartz, B. C.-K. Tee, J. Mei, A. L. Appleton, D. H. Kim, H. Wang, Z. Bao, *Nat. Commun.* **2013**, *4*, 1859.

[35] M. Amjadi, A. Pichitpajongkit, S. Lee, S. Ryu, I. Park, *ACS Nano* **2014**, *8*, 5154.

[36] V. Nguyen, R. Zhu, R. Yang, *Nano Energy* **2015**, *14*, 49.

[37] R. V. Martinez, C. R. Fish, X. Chen, G. M. Whitesides, *Adv. Funct. Mater.* **2012**, *22*, 1376.

[38] T. Li, J. Zou, F. Xing, M. Zhang, X. Cao, N. Wang, Z. L. Wang, *ACS Nano* **2017**, *11*, 3950.